Estimation of surface ammonia concentrations and emissions in China from the polar-orbiting Infrared Atmospheric Sounding Interferometer and the FY-4A Geostationary Interferometric Infrared Sounder

Pu Liu[1], Jia Ding[1], Lei Liu[1], Wen Xu[2], Xuejun Liu[2]

[1] School of Earth and Environmental Sciences, Lanzhou University, Lanzhou, 730000, China

[2] College of Resources and Environmental Sciences, Centre for Resources, Environment and Food Security, Key Lab of Plant-Soil Interactions of MOE, China Agricultural University, Beijing 100193, China

Correspondence to: Lei Liu (liuleigeo@lzu.edu.cn)

Abstract

Ammonia (NH_3) is the most important alkaline gas in the atmosphere, which has negative effects on biodiversity, ecosystems, soil acidification and human health. China has the largest NH_3 emissions globally, mainly associated with agricultural sources including nitrogen fertilizer and livestock. However, there is still a limited number of ground monitoring sites in China, hindering our understanding of both surface NH_3 concentrations and emissions. In this study, using the polar-orbiting satellite (IASI) and Fengyun-4 geostationary satellite (GIIRS), we analyzed the changes of hourly NH_3 concentrations, and estimated surface NH_3 concentrations and NH_3 emissions in China. GIIRS-derived NH_3 concentrations in the daytime were generally higher than that at night, with high values during 10:00-16:00. Satellite-derived surface NH_3 concentrations were generally consistent with the ground observations with R-square

21 at 0.72 and slope equal to 1.03. Satellite-based NH_3 emissions ranged from 12.17-17.77 Tg N yr^{-1} during

22 2008-2019. Spatially, high values of NH_3 emissions mainly occurred in the North China Plain, Northeast

23 China and Sichuan Basin, while low values were mainly distributed in western China (Qinghai-Tibet

24 Plateau). Our study shows a high predictive power of using satellite data to estimate surface NH_3

25 concentrations and NH_3 emissions over multiple temporal and spatial scales, which provides an important

26 reference for understanding NH_3 changes over China.

27 **1 Introduction**

28 Ammonia (NH_3) is a highly active gas in the atmosphere and the most important alkaline gas, playing an

29 important role in atmospheric chemistry (Fowler et al., 2013). NH_3 reacts with acid pollutants (SO_2 and

30 NO_x) to form fine particulate matters, such as PM2.5, leading to haze pollution. In addition, the deposition

31 of NH_3 and NH_4^+ could also cause environmental problems such as water eutrophication, biodiversity

32 loss and soil acidification (Paerl et al., 2014). China has become a major region for NH_3 emissions

33 globally, because of rapid growth of population and agricultural production (Zhang et al., 2017; Liu et al.,

34 2022). To provide a scientific basis for dealing with NH_3 pollution, it is urgent to accurately estimate both

35 surface NH_3 concentrations and emissions in China.

36

37 Surface NH_3 concentrations can be estimated by ground measurements and model simulations. Ground

38 measurements are considered to be the most accurate quantitative method. Current national NH_3

39 observation networks in China include the National Nitrogen Deposition Monitoring Network (NNDMN)

40 established by China Agricultural University (Xu et al., 2015) and the Ammonia Monitoring Network

(AMoN-China) established based on the Chinese Ecosystem Research Network (CERN) (Pan et al., 2018). The NNDMN can measure ground NH_3 concentrations since 2010, while the AMoN-China only makes the measurements in 2015-2016. The above two monitoring networks both monitor surface NH_3 concentrations on a monthly basis, and lack monitoring of the hourly NH_3 changes. Some studies have conducted research on the intra-day/hourly changes of NH_3 concentrations based on ground observations. Werner et al. (2017) measured hourly NH_3 concentration in 2012 at the Harwell site in the United Kingdom, and found that high NH_3 concentration usually occurred in the afternoon. Similarly, Kutzner et al. (2021) observed the hourly NH_3 concentration on the SIRTA Observatory in Paris and found NH_3 concentration was highest in the late afternoon. Pandolfi et al. (2012) studied the day-night cycle of NH_3 concentration at the two stations in Barcelona in summer, and found that the NH_3 concentration was highly associated with local meteorology and traffic emissions. However, there are still a limited number of monitoring sites on the hourly NH_3 changes in China.

Agricultural fertilizer and livestock production have led to a large amount of NH_3 emissions. China's cultivated land area accounts for less than 10% of the world, but it consumes about 30% of the world's nitrogen (N) fertilizer (Peng et al., 2002). Estimation of NH_3 emissions is mainly based on a bottom-up method, using NH_3 source statistics (fertilization, animal husbandry, etc.) and emission factors. Zhou et al. (2016) calculated the annual farmland NH_3 emission (3.96 ± 0.76 Tg N yr^{-1}) over China in 2008 based on the bottom-up method, which was 40% higher than the emission in the Intergovernmental Panel on Climate Change (IPCC) Tier 1 guidelines (2.89 Tg N yr^{-1}). Zhang et al. (2017) reassessed China's NH_3 emissions based on the mass balance method, and found NH_3 emissions increased from 12.1 ± 0.8 in 2000

to 15.6 ± 0.9 Tg N yr^{-1} in 2015, with an annual growth rate of 1.9% . Fu et al. (2020) estimated that China's NH$_3$ emissions increased from 4.7 in 1980 to 11 Tg N yr^{-1} in 2016. Although many studies regarding NH$_3$ emissions have been carried out in China, great uncertainties and large ranges (7-16 Tg N yr^{-1}) still existed in the estimates of China's NH$_3$ emissions (Dong et al., 2010; Huang et al., 2012; Kang et al., 2016).

Besides the bottom-up estimates, some studies used data assimilation methods by ground monitoring data to constrain NH$_3$ emission estimates. Paulot et al. (2014) assimilated the GEOS-Chem with ground observations of wet N$_r$ deposition, and estimated China's NH$_3$ emission as 8.4 Tg N yr^{-1} in 2008 with seasonal NH$_3$ emission peaked in summer. Gilliland et al. (2003) used the data assimilation method by the air quality model (CMAQ) with the wet NH$_4^+$ concentration data from the USA National Atmospheric Deposition Program Network, and found that obvious seasonal differences appeared in NH$_3$ emissions linked to N fertilizer and temperature. Kong et al. (2019) carried out inversion through assimilating surface AMoN NH$_3$ observation data, and improved the accuracy of temporal and spatial pattern of NH$_3$ emissions in China.

In recent years, atmospheric remote sensing has developed rapidly, which can monitor NH$_3$ at a global scale including the polar-orbiting satellite instruments such as the Tropospheric Emission Spectrometer (TES), Infrared Atmospheric Sounding Interferometer (IASI), Cross-track Infrared Sounder (CrIS), Atmospheric Infrared Sounder (AIRS), and Greenhouse Gases Observing Satellite (GOSAT) (Someya et al., 2020). Many studies have reported the effectiveness of using satellite data to study NH$_3$ dynamics.

83 Pinder et al. (2011) found that TES observation can capture spatial-temporal NH_3 patterns compared with

84 surface measurement; Van Damme et al. (2014) studied the seasonal and annual NH_3 changes in the

85 northern and southern hemisphere using the IASI NH_3 column data, and found that the seasonality in the

86 southern hemisphere is mainly related to biomass burning; Shephard and Cady-Pereira (2015) developed

87 the CrIS NH_3 inversion algorithms, and found that CrIS can capture the global spatial distribution of NH_3

88 concentration; Warner et al. (2016) identified the main hotspots of agricultural NH_3 regions using AIRS,

89 such as South Asia, China, the United States and some parts of Europe, and found that NH_3 concentrations

90 increased at these agricultural regions since 2003. Besides, some studies also used the satellite

91 measurements to improve the estimates of NH_3 emissions. Zhang et al. (2017) developed a top-down

92 inversion method using TES NH_3 observation to quantify China's NH_3 emission, and obtained annual

93 NH_3 emission as 11.7 Tg N yr^{-1} in 2008. Marais et al. (2021) estimated NH_3 emissions in the UK based

94 on IASI and CrIS and found the relative errors of IASI-derived NH_3 emissions were 11-36% and 9-27%

95 respectively; Van Damme et al. (2018) used the high-resolution IASI NH_3 maps to identify, classify and

96 quantify NH_3 emission hotspots in the world, which was helpful to understand the man-made point NH_3

97 sources; Dammers et al. (2019) identified global 249 NH_3 emission point sources based on CrIS, whose

98 total emission was about 2.5 times higher than that reported in the HTAPv2 emissions.

99

100 Besides the polar-orbiting satellite, China's Geostationary Interferometric Infrared Sounder (GIIRS)

101 onboard the Chinese FY-4A satellite can measure hourly changes of atmospheric NH_3 almost all of Asia

102 per day, which provides great potential to study the diel cycle of NH_3. In this study, GIIRS is used to

103 study the NH_3 diel cycle (hourly changes), which is essential for understanding the differences between

different times in a day by the polar-orbiting satellites (such as IASI at 9:30 and CrIS at 13:30). Second, the surface NH_3 concentration in China is estimated based on both GIIRS and IASI, which is then compared with the NNDMN. Third, NH_3 emission in China is calculated based on satellite-derived surface NH_3 concentration and the feedback relationship between surface NH_3 concentration and emission by a chemistry transport model (GEOS-Chem). Finally, the spatial-temporal characteristics of satellite-derived surface NH_3 concentration and emission are analyzed, and the uncertainties are discussed.

2 Data and methods

2.1 Satellite GIIRS NH_3

The Geostationary Interferometric Infrared Sounder (GIIRS) onboard the Fengyun-4A geostationary satellite (FY-4A) launched by China in 2016 is the world's first hyperspectral atmospheric infrared sounder. The FY-4A GIIRS detected spectral range is 700-2250 cm^{-1}, including 1648 spectral channels and 14 radiations imaging channels, covering visible light, short, medium and long wave infrared bands. The spatial resolutions of the detector are 2.0 km in the visible bands and 16 km in the infrared bands. It covers almost the whole of Asia and scans 10 times a day. The GIIRS can detect the temperature and humidity profiles and trace gases at high frequencies.

NH_3 has two large absorption characteristics in the long wave infrared (about 930 cm^{-1} and 965 cm^{-1}). The contribution of NH_3 to the brightness temperature of these two bands is between 2-4 k. The core of inversion algorithms is based on the so-called hyperspectral radiation index (HRI), which quantifies the spectral characteristics of NH_3. The HRI index depends on whether the satellite instrument detects the

124 presence of NH₃. The average value of HRI is 0 with a standard deviation of 1, and the HRI range is [-

125 1,1]. The algorithm for estimating IASI NH₃ column concentration is to convert HRI into a column using

126 the so-called neural network (Clarisse et al., 2021).

127

128 In this study, we use hourly NH₃ concentrations during 2019-2020 (from November 2019 to October

129 2020) to study NH₃ diel cycle with a resolution of 0.5°. The original data is in H5 format, and the unit of

130 NH₃ is molecules cm^{-2}. The data is processed with MATLAB software. First, observations with

131 considerable uncertainties (relative error exceeds 50%) and high clouds (cloud cover exceeds 20%) are

132 removed (Fig. S1a). Secondly, the world standard time (UTC) by GIIRS is converted to local time, and

133 the data in H5 format is converted to TIFF data.

134 **2.2 Satellite IASI NH₃**

135 IASI instrument is on board the polar solar synchronous Metop-A platform. It has been running stably

136 since 2006 to measure the infrared radiation emitted by the earth (Van Damme et al., 2014). IASI can

137 measure the infrared radiation emitted by the earth's surface and atmosphere in the spectral range of 645-

138 2760 cm^{-1}. It can observe the world twice a day, and cross the equator at 9:30 and 21:30 local time, with

139 a spatial resolution of 12 km at nadir. However, only daytime satellite measurements are used, because

140 nighttime measurements usually have greater uncertainties related to thermal contrasts (Van Damme et

141 al., 2017).

142 The near-real time dataset of the total NH₃ column (ANNI-NH₃-v3) was used here. The properties of IASI

143 NH₃ data include NH₃ column concentration, longitude, latitude, measurement time, cloud cover,

144 uncertainty, solar zenith angle and other parameters. The daily NH₃ column from 2008 to 2019 was used.

145 The format of the original data is NC format, and the unit is mol cm^{-2}. The observation data with cloud

146 cover larger than 20% and the uncertainty above 50% were removed (Fig. S1b). We gridded the data to

147 0.1° by using the arithmetic average methods.

148 **2.3 Ground NH$_3$ measurements**

149 Surface NH$_3$ concentrations in the NNDMN were used to compare with the satellite estimates including

150 43 observation stations. The land types of the NNDMN sites cover cities, farmland, coastal areas, forests

151 and grasslands. Measurements during the period from January 2010 to December 2015 by the NNDMN

152 were used. Surface NH$_3$ concentrations were measured using an active DELTA (DEnuder for Long-Term

153 Atmospheric sampling) (Flechard et al., 2011). For the hourly measurements, we collected the data from

154 the published papers including 5 sites (Table S1) including Xianghe (39.75 °N, 116.96 °E, 2017.12 -

155 2018.2) (He et al., 2020), Fudan University (31.30 °N, 121.50 °E, 2013.7.1-2014.9.30) (Wang et al.,

156 2015), Dianhushan (31.09 °N, 120.98 °E, 2014.3.1-2014.6.30) (Wang et al., 2015), Jinshan Chemical

157 Industry Park (30.73 °N, 121.27 °E, 2014.1.6-2014.6.30) (Wang et al., 2015), and Gucheng (39.15 °N,

158 115.73 °E, 2016.3-2017.5) (Kuang et al., 2020). The Xianghe site in Hebei Province and Dianhushan site

159 in Shanghai represent rural environments; Jinshan Chemical Industry Park represents industrial

160 environments; Gucheng site in Hebei and the Fudan University site in Shanghai represent urban

161 environments.

162 **2.4 GEOS-Chem**

163 The GEOS-Chem model version 12.3.0 is a three-dimensional chemistry transport model developed by

164 Harvard University, which has been widely used in the field of atmospheric studies (Eastham et al., 2014).

165 The nested regional model in Asia was used in this study driven by assimilated GEOS-5 meteorological

166 data at a horizontal resolution of $1/2° \times 2/3°$. Dry deposition calculation in GEOS-Chem follows a

167 standard resistance-in-series model (Wesely, 2007), while wet deposition includes both convective

168 updraft and large-scale precipitation scavenging (Jacob, 1999). The GEOS-Chem model here does not

169 consider land-atmosphere bi-directional NH_3 exchange, and the NH_3 flux was parameterized as uncoupled

170 emission and dry deposition processes. Anthropogenic emissions over China were from the Regional

171 Emission in Asia (REAS-v2) inventory. The GEOS-Chem outputs of NH_3 concentrations include 47

172 layers from the ground to the top of atmosphere, which were used to capture NH_3 vertical profiles. The

173 feedback between surface NH_3 concentration and emissions was also calculated by GEOS-Chem.

174 **2.5 Satellite-based surface NH₃ estimates and emissions**

175 Surface NH_3 concentrations were estimated using the satellite NH_3 columns as well as NH_3 vertical

176 profiles. To gain the continuous vertical NH_3 profile, the Gaussian function was used to fit the 47 layers'

177 NH_3 concentrations. A three parameter Gaussian function was used to fit NH_3 vertical profiles at each

178 grid box from GEOS-Chem according to previous studies (Liu et al., 2019).

179
$$\rho(Z) = \sum_{i=1}^{n} \rho_{max,i} e^{-(\frac{Z-Z_{0,i}}{\sigma_i})^2} , \tag{1}$$

180 where Z is the height of a layer in the atmospheric chemical transport modeling (ACTM); ρ_{max}, Z_0 and σ

181 are the maximum of NH_3 concentration, the corresponding height with the maximum of NH_3

182 concentration and the thickness of NH_3 concentration layer (one standard error of Gaussian function).

183

184 The satellite-derived NH_3 concentration at the height of h_G can be calculated as:

$$S_{G\_NH_3} = S_{trop} \times \frac{\rho(h_G)}{\int_0^{h_{trop}} \rho(Z)dx} \times \frac{G_{ACTM}^{1-24}}{G_{ACTM}^{overpass}}, \tag{2}$$

where $\frac{\rho(h_G)}{\int_0^{h_{trop}} \rho(Z)dx}$ represents the ratio of NH_3 concentration at the height of h_G to total columns

($\int_0^{h_{trop}} \rho(Z) \, dx$); S_{trop} represents satellite-derived NH_3 columns; $\frac{G_{ACTM}^{1-24}}{G_{ACTM}^{overpass}}$ is the ratio of average surface

NH_3 concentration (G_{ACTM}^{1-24}) to that at satellite overpass time ($G_{ACTM}^{overpass}$) by an ACTM.

The mass balance method (Lamsal et al., 2011; Geddes and Martin, 2017; Cooper et al., 2017) was used to exploit the feedback ratio of surface NH_3 concentrations and NH_3 emissions (Marais et al., 2021):

$$E_s = S_{G\_NH_3} \times \left(\frac{E}{G_{G\_NH_3}}\right)_m, \tag{3}$$

where E_s is satellite-based NH_3 emissions; $S_{G\_NH_3}$ is the satellite-derived surface NH_3 concentrations;

$\left(\frac{E}{G_{G\_NH_3}}\right)_m$ is the ratio of surface NH_3 concentrations and NH_3 emissions simulated by the GEOS-Chem.

3 Results and discussions

3.1 GIIRS-based hourly NH₃ concentrations during 2019-2020

Fig. 1 shows the hourly NH_3 concentrations observed from GIIRS during 2019-2020. Daytime NH_3 columns were significantly higher than those at night. The intra-day hourly NH_3 columns showed an overall increase first, then a decrease, with high values during 10:00-17:00. The increase in temperature enhanced the volatilization of NH_3, which may explain high values of NH_3 concentrations during the daytime.
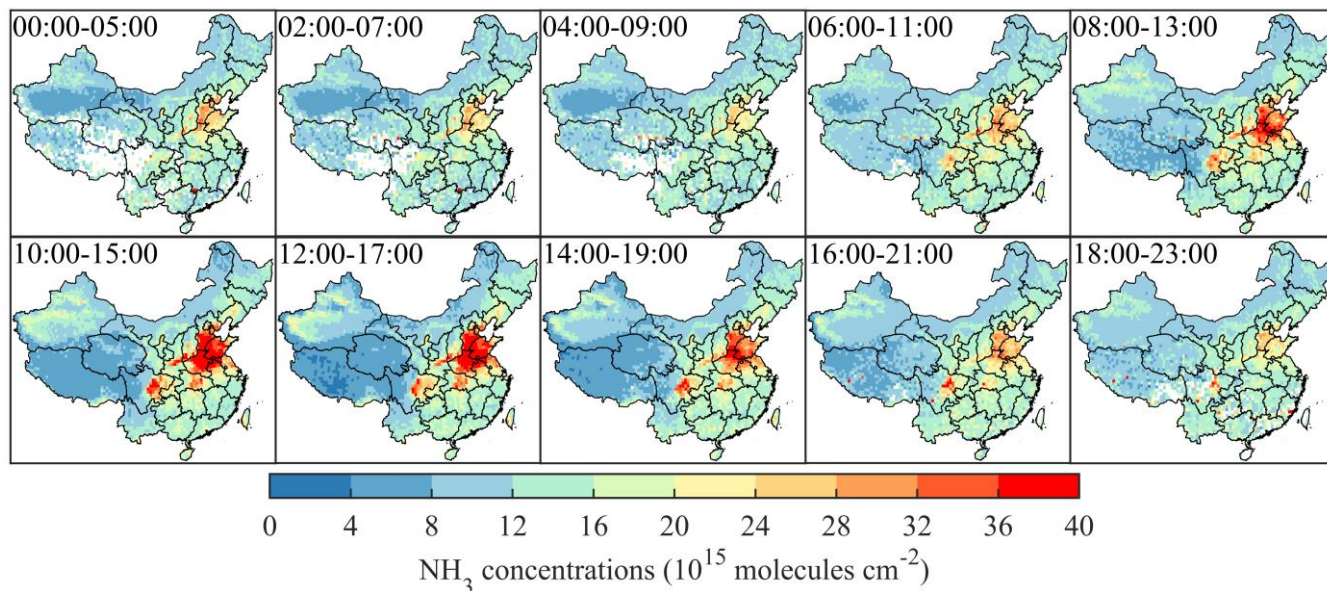
Figure 1. Monthly average NH₃ concentrations for each of the 10 GIIRS overpass time periods during 2019-2020.

Ground-based measurements of hourly NH$_3$ concentrations are very lacking, and the timespan may be different from GIIRS measurements. Here we only used them to show the hourly patterns of NH$_3$ concentrations (Fig. 2). The Xianghe site in Hebei Province and Dianhushan site in Shanghai represent rural environments; Jinshan Chemical Industry Park represents industrial environments; Gucheng site in Hebei and the Fudan University site in Shanghai represent urban environments.

NH$_3$ concentration in the rural environment basically shows a normal distribution, and high NH$_3$ concentration generally appears between 10:00-16:00, which may be related to agricultural activities and temperature. In the industrial environment (Jinshan Chemical Industry Park, JSP), NH$_3$ concentration fluctuates irregularly, and two peaks appear at 12:00 and 6:00-8:00, while NH$_3$ concentration tends to be stable at other times. In the urban environment, the changes in NH$_3$ concentration by satellite at the Gucheng site are more consistent with ground monitoring, showing a clear peak around 9:00-13:00; NH$_3$

216 concentration at the Fudan University site gradually decreases from the morning peak to the afternoon.

217 The evaporation of dew may drive the NH₃ increase from the morning to the noon (Wang et al., 2015).

218 NH₃ concentration in cities (Gucheng and Fudan University) has double peaks between 6:00-8:00 and

219 18:00-19:00, which may also be related to traffic emissions. In summary, except for industrial sites, hourly

220 NH₃ in China has a large variability between day and night and the hourly NH₃ patterns are affected by

221 many factors, of which anthropogenic emissions and temperature seem to be the most important driving

222 factors.

223
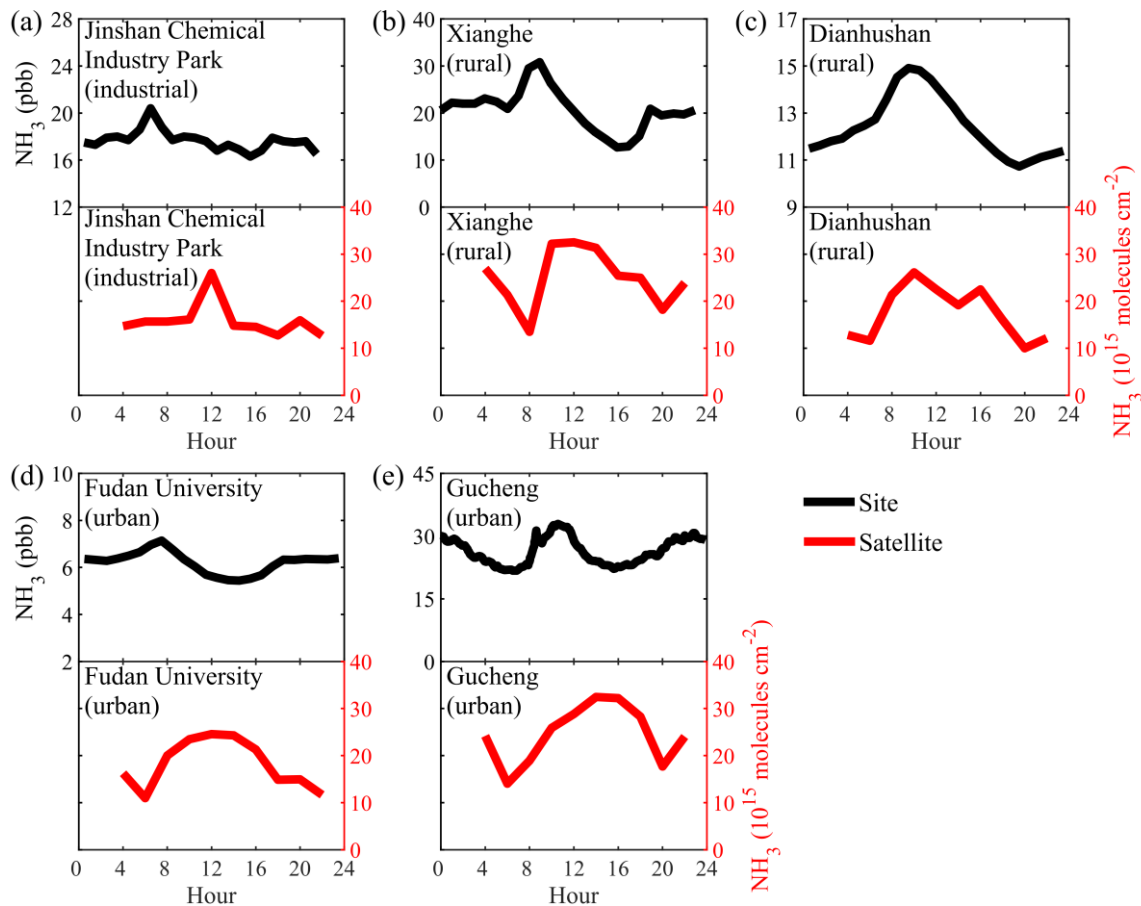
Figure 2. GIIRS-based and measured hourly NH₃ concentrations at five sites including Jinshan Chemical

Industry Park (JSP, a), Xianghe (XH, b), Dianhushan (DSL, c), Fudan University (FDU, d) and Gucheng

226 (GC, e).

227

228 Spatial distribution of GIIRS-based surface NH$_3$ concentrations across China had large variability. High

229 surface NH$_3$ concentration (>10 μg N m^{-3}) is mainly concentrated in the North China Plain (NCP),

230 followed by the Sichuan Basin, Northeast China and parts of Xinjiang, while low values (<4 μg N m^{-3})

231 are mainly concentrated in the Qinghai-Tibet Plateau. High surface NH$_3$ concentration (126.85 μg N m^{-3})

232 appears in July (6.78 μg N m^{-3} as average), and the lowest value (0.23 μg N m^{-3}) appears in November

233 (3.25 μg N m^{-3} as average). There are obvious seasonal changes in surface NH$_3$ concentrations in the NCP

234 with high values in summer, and low values in winter, related to both agricultural N fertilizer and higher

235 temperature.
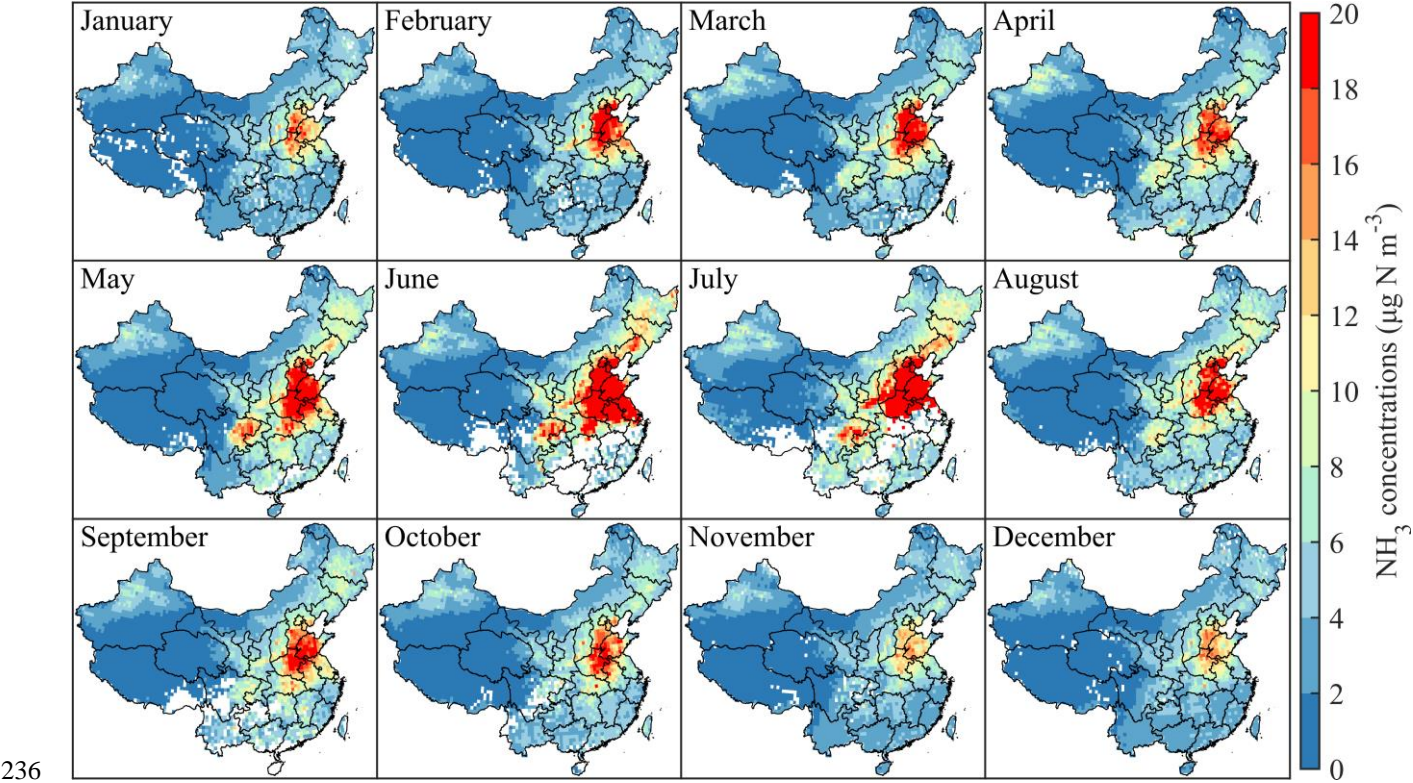
237 **Figure 3.** Spatial distribution of monthly surface NH$_3$ concentrations in China by GIIRS in 2019-2020.

3.2 IASI-based NH₃ surface concentrations

The observation data of the NNDMN in China was collected to compare with IASI-derived surface NH₃ concentration. In general, a good consistency was found between measurements and satellite estimates with the regression R^2 as 0.72 and the RMSE as 2.24 µg N m⁻³. The coefficient of the fitted line was 1.03≈1 and the bias was 2.59%.
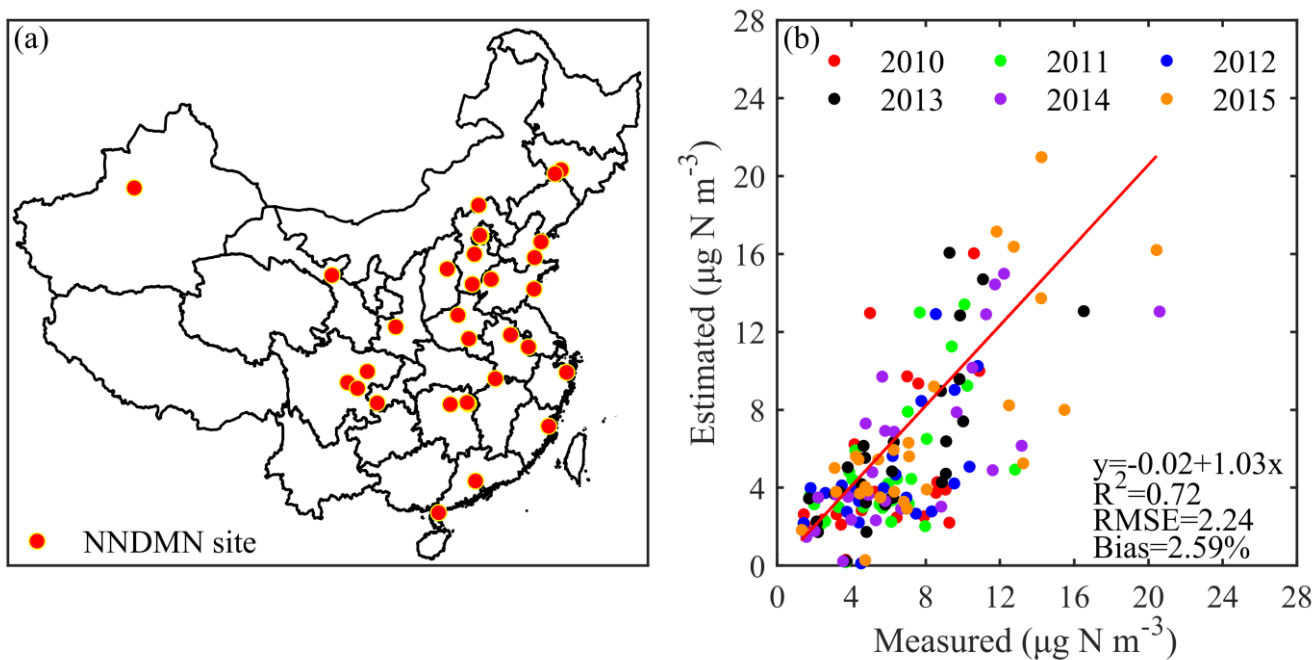
Figure 4. Comparison of IASI surface NH₃ concentrations with NNDMN measurements. (a) The locations of NNDMN; (b) the regression results between satellite-estimates and measurements.

Monthly regression R^2 between the satellite-derived NH₃ concentration and the measured NH₃ was 0.38- 0.84. The regression R^2 reached the higher value (>0.80) in July and August. The RMSE ranged from 2.29- 3.36 µg N m⁻³, which reached the maximum value of 3.36 µg N m⁻³ in July, and reached the smallest in March (2.29 µg N m⁻³). The bias is basically less than 31% for all months, and reached the minimum

251 value of 0.67% in February, indicating that the monthly IASI-derived surface concentration obtained are

252 consistent with measurements.

253
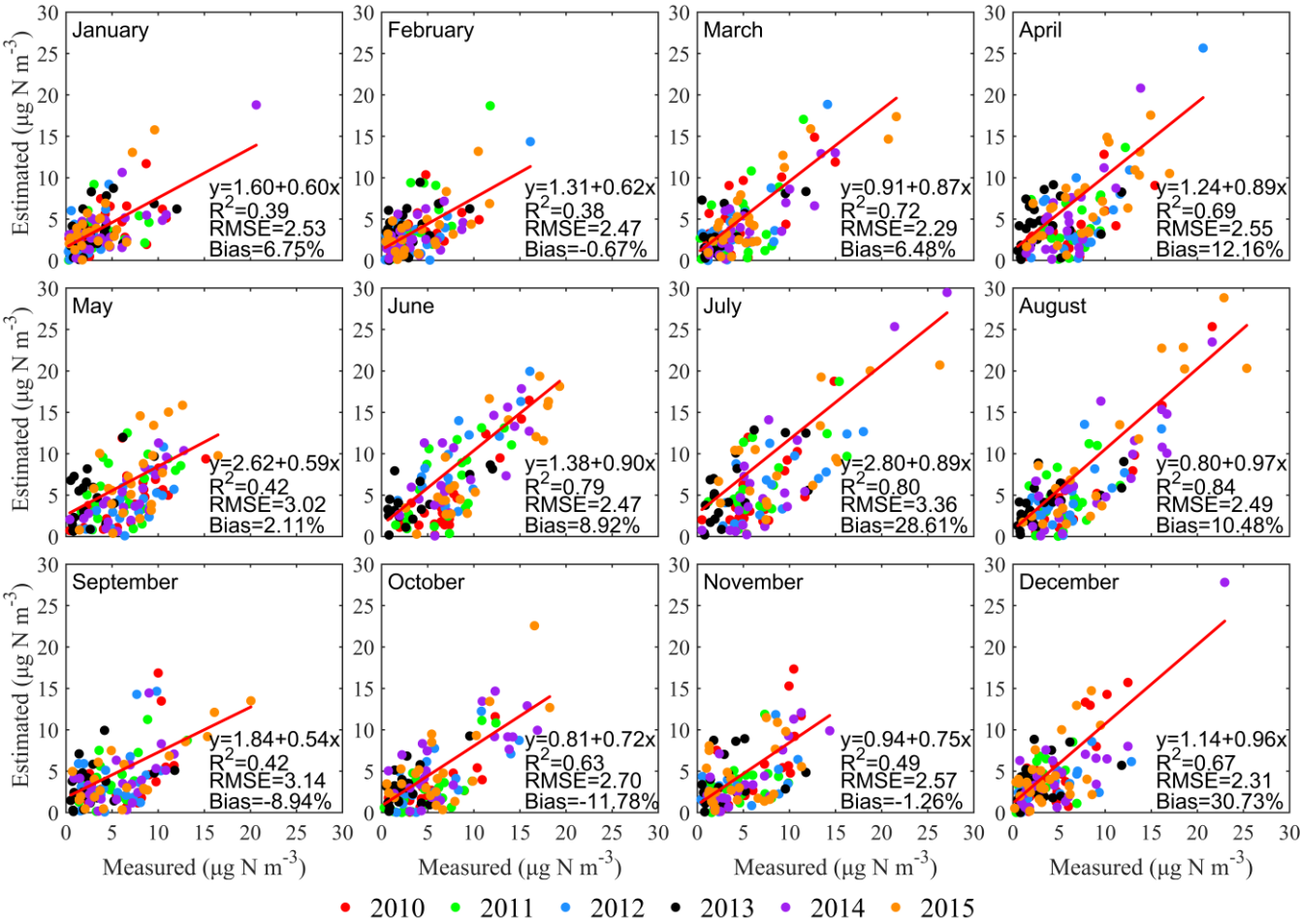
Figure 5. Comparison of monthly average values of IASI-derived and observed NH₃ surface

255 concentrations in 2010-2015.

256

257 Fig. 6 shows the monthly changes of surface NH₃ concentrations in Huinong County in Ningxia from

258 2010 to 2015 for a total of 72 months. Surface NH₃ concentrations retrieved by IASI were compared with

259 the observation data at Huinong. The highest value of each year basically appeared from June to August,

and the lowest values appeared from December to January. In the past 6 years, the maximum measured

NH$_3$ concentration appeared in June 2015 (18.9 µg N m^{-3}), and the minimum appeared in November 2012

(0.6 µg N m^{-3}). The observation data and satellite data have the same seasonal changes.
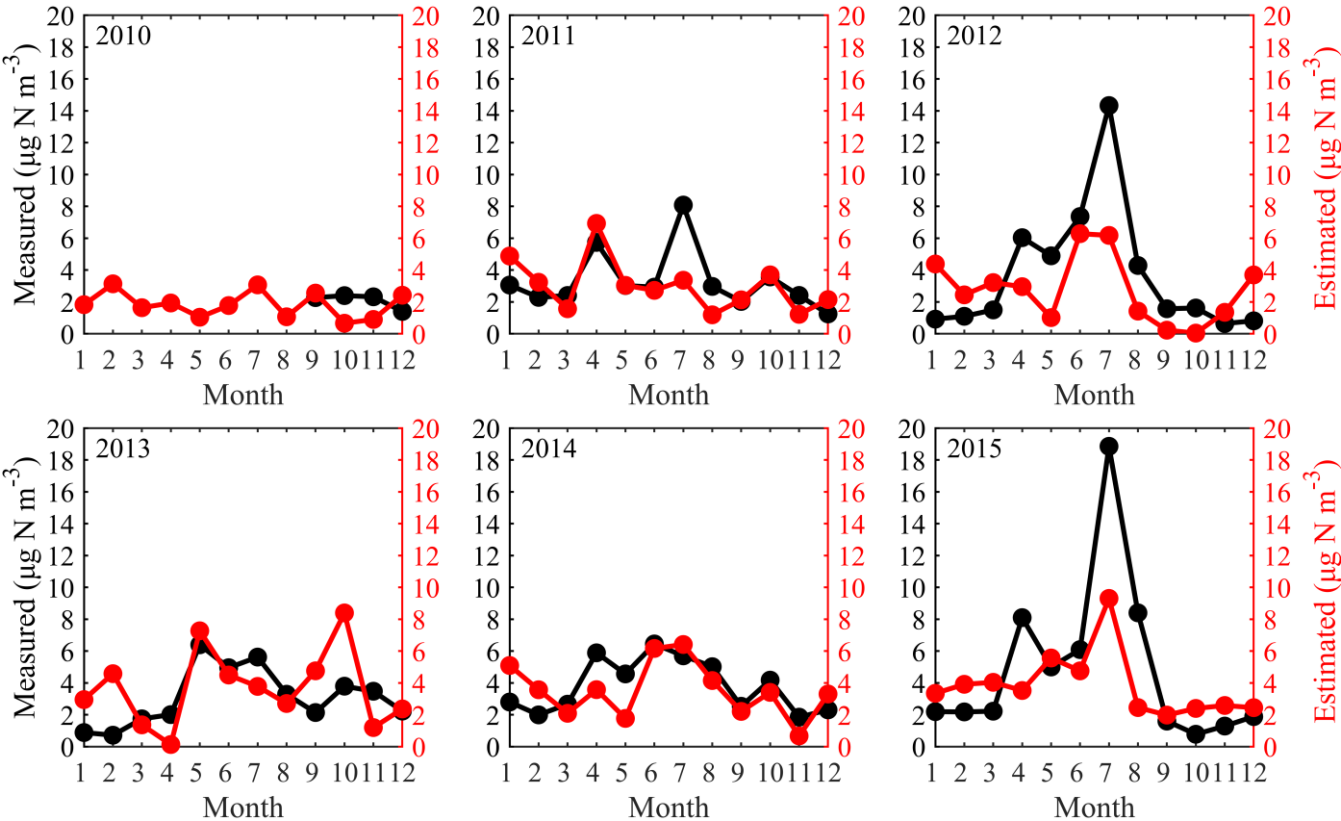
Figure 6. Monthly changes of NH$_3$ concentrations in Huinong County in Ningxia from 2010 to 2015 for

a total of 72 months during 2010-2015.

Fig. 3 and Fig. 7 show the spatial distribution of GIIRS-derived and IASI-derived surface NH$_3$

concentrations in 2019. The spatial distribution and gradients of surface NH$_3$ concentrations by the GIIRS

and IASI have the same gradients from eastern to western regions. One notable difference occurred in the

270 middle and lower reaches of the Yangtze River in June and July since the GIIRS observations are affected

271 by clouds and had missing data.

272
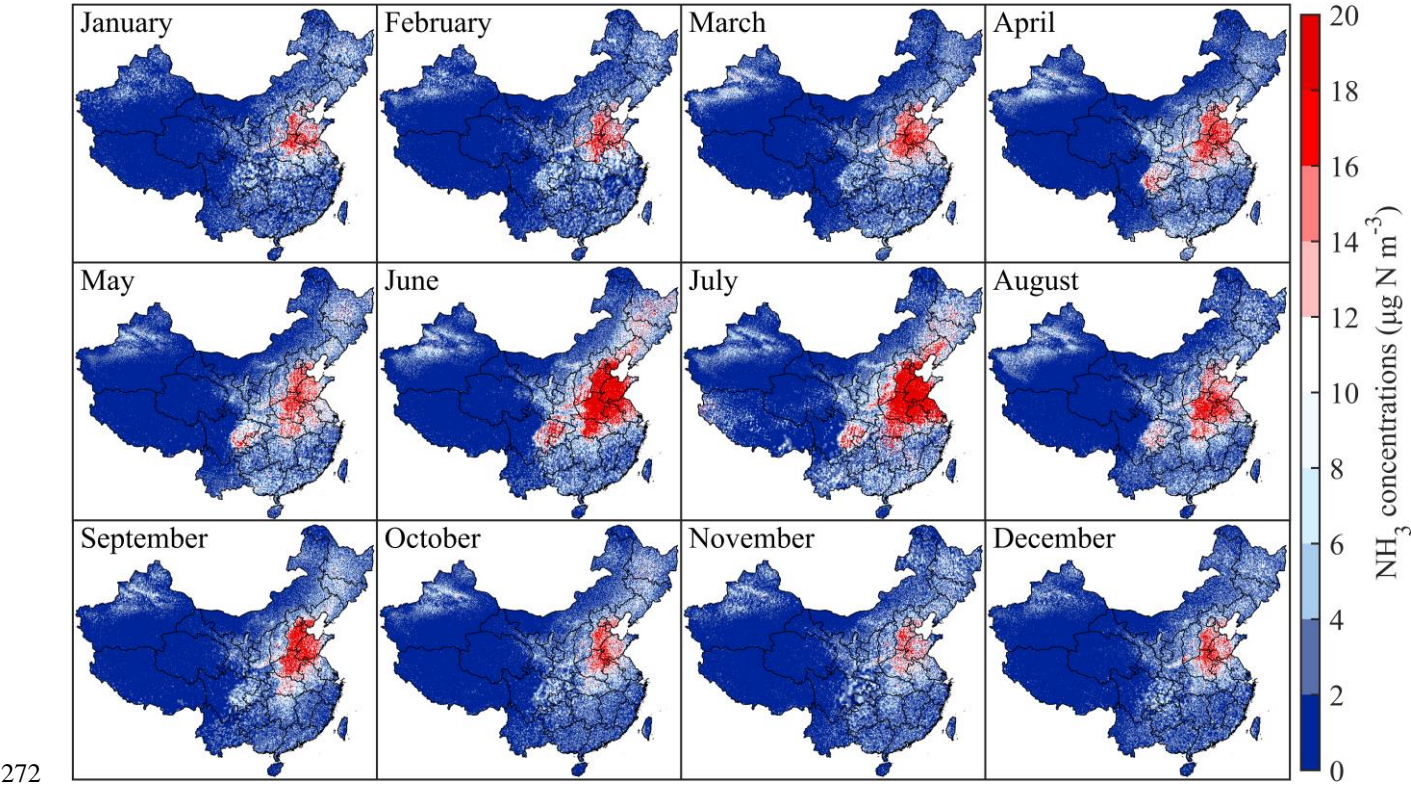
Figure 7. Spatial distribution of monthly surface NH₃ concentrations in China by IASI in 2019.

274

275 **3.3 IASI-derived NH₃ emissions**

276 Based on the top-down estimates, China's NH₃ emissions ranged from 12.17-17.77 Tg N yr^{-1} during

277 2008-2019. From 2008 to 2015, NH₃ emissions increased from 13.00 Tg N yr^{-1} to 17.06 Tg N yr^{-1}. Since

278 2008, the temperature in China has risen steadily (Ding et al., 2007), promoting the volatilization of NH₃,

279 which partly explains the increase in NH₃ emissions from 2008 to 2015. After 2015, NH₃ emissions

280 fluctuated and changed slightly (16.08-17.77 Tg N yr^{-1}). Compared with other studies, the change in NH₃

281 emissions from 2008 to 2015 is consistent with previous estimates, and the overall NH₃ emissions show

282 an upward trend (Kang et al., 2016; Zhang et al., 2018; Ma, 2020; Fu et al., 2020; Zhang et al., 2021).

283 Our estimates are on the rise as a whole, but the calculated values are generally lower than those by Fu et

284 al. (2020) (around 15 Tg N yr^{-1}), but larger than those by EDGAR and Kang et al. (2016).

285

286 In terms of spatial distribution, high NH_3 emissions are generally distributed in the North China Plain,

287 Sichuan Basin, Northeast China and Xinjiang, while the low values are mainly distributed in the

288 Southwest China (especially Qinghai-Tibet Plateau). The North China Plain is China's granary, with

289 developed agriculture and animal husbandry, high population densities and strong human activities

290 (including vehicle emissions) (Zhang et al., 2006; Wang et al., 2020). In contrast, South China is rich in

291 rainfall, which promotes the deposition of NH_3 and suppresses its volatilization to a certain extent.

292

293 The spatial distribution of NH_3 emissions in January, April, July and October were selected to characterize

294 the seasonal variations. The average emissions for the four months were 1.15 kg N ha^{-1}, 1.31 kg N ha^{-1},

295 2.31 kg N ha^{-1} and 1.16 kg N ha^{-1} in January, April, July and October, indicating that NH_3 emission is the

296 highest in summer and the lowest in winter. The annual average emission intensity of 2019 is 16.53 kg N

297 ha^{-1} (0.09-313.47 kg N ha^{-1}). Fig. 8b shows the monthly changes in NH_3 emissions, which basically shows

298 a normal distribution. High values are generally distributed in June and July, and low values are generally

299 distributed in November and December. It reached the maximum monthly emission of 2.6 Tg N m^{-1} in

300 July 2019 and reached the minimum monthly emission in November and December (1.1 Tg N m^{-1}).

301
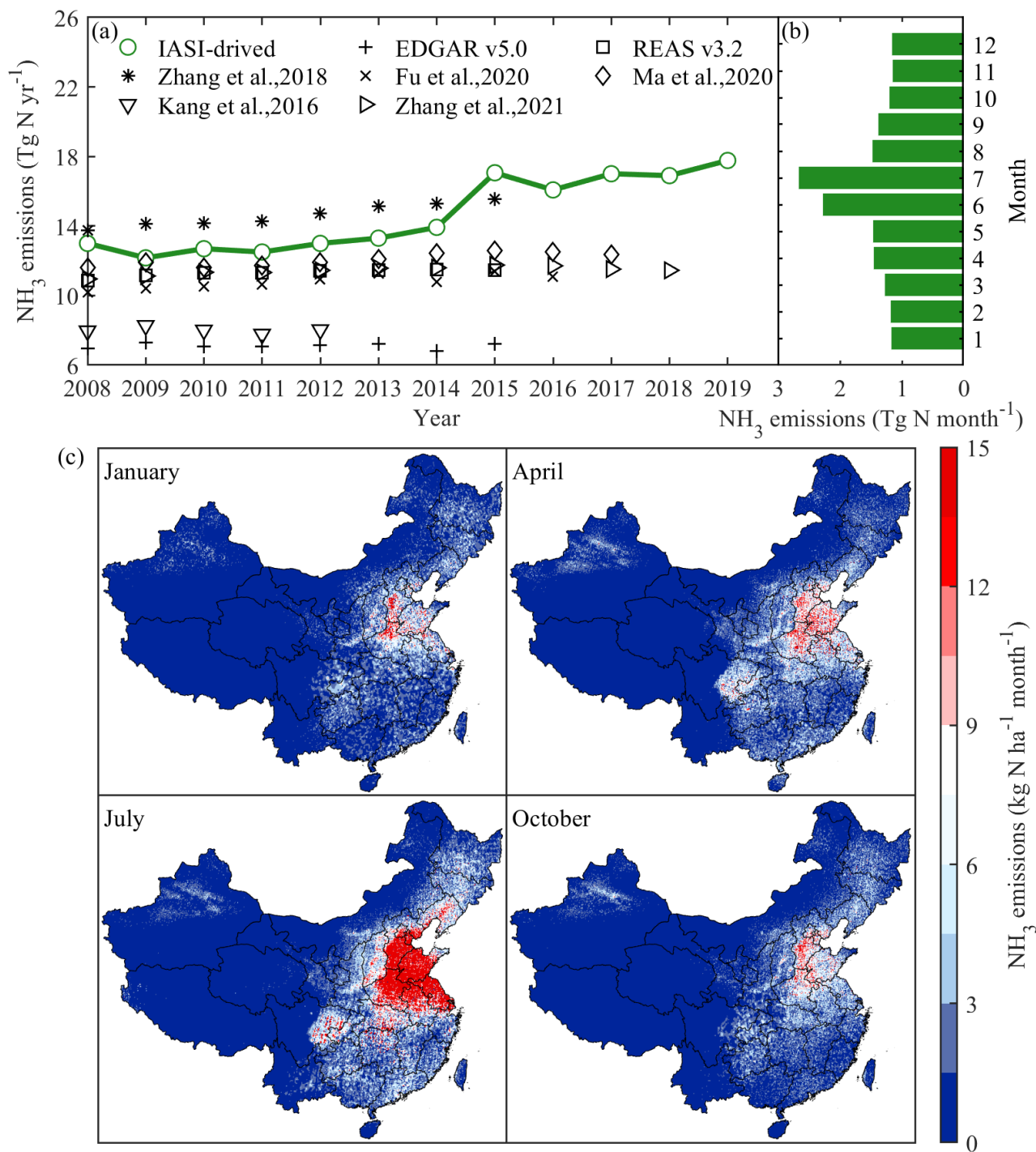
Figure 8. Annual changes of NH₃ emissions (a), monthly changes of NH₃ emissions in 2019 (b) and spatial distribution of NH₃ emissions by month in 2019 (c).

4 Limitations and outlook

This study developed satellite-based surface NH_3 concentration and emissions in China based on remote sensing data (IASI and GIIRS). However, several limitations have been identified in this study. First, the Fengyun geostationary satellite used in this study can achieve hourly NH_3 concentrations, but the time series is still very short (2019.11-2020.10), and satellite observations are affected by clouds and meteorological conditions, resulting in missing values in parts of the Yangtze River Basin.

Second, we used a relatively fixed average conversion ratio (Fig. S2) to estimate surface NH_3 concentrations and NH_3 emissions in China, ignoring the time-series variation of the ratio, due to the temporal constraint of emission inventory. In this case, non-emission factors led to higher satellite observed NH_3 column, for example, emission reductions of SO_2 and NO_2 led to increased NH_3 column (Lachatre et al., 2019; Fu et al., 2020), which can introduce uncertainty into NH_3 emission calculations using concentration as the main parameter.

Third, the spatial resolution of the NH_3 vertical profile simulated by the atmospheric model is relatively coarse (0.5 degrees). In order to make it consistent with the spatial resolution of the remote sensing data, the outputs of GEOS-Chem (vertical profiles and feedback ratio between emissions and surface NH_3 concentrations) were interpolated through resampling methods. Owing to the resolution limit, the ratio-based mass balance approach to estimate NH_3 emissions neglected the effects of internal transport of NH_3 and displacement of emission sources within the fine grid.

326 Finally, there are some uncertainties and biases in the observed NH$_3$ column by satellite. Earlier versions

327 of the IASI NH$_3$ column product were 25-50% lower than ground-based measurements (Whitburn et al.,

328 2016; Dammers et al., 2017). However, the new version of IASI v3 lacks a comprehensive ground-based

329 measurement assessment, which has only been compared with limited aircraft observations (Guo et al.,

330 2021). Comparing IASI-derived surface NH$_3$ concentrations with measurements of ground sites

331 (NNDMN) generally shows consistency in this study. The further work is needed for the complete

332 assessment and error analysis.

333

334 At present, there are more and more satellite sensors (GOSAT, CrIS, AIRS, etc.) that can monitor NH$_3$

335 concentrations. This study only used IASI and GIIRS, and in the future, data from different satellites can

336 be merged to analyze NH$_3$ changes on multiple temporal and spatial scales.

337 **5 Conclusion**

338 We use GIIRS to study the NH$_3$ diel cycle, and estimate surface NH$_3$ concentrations and emissions based

339 on IASI in China. There are obvious hourly changes in NH$_3$ concentration in China using GIIRS. Overall,

340 NH$_3$ concentrations are larger in the daytime than at nighttime in China. Hourly NH$_3$ concentrations at

341 different land use show different patterns, but high values generally appear in 10:00-16:00. Comparing

342 IASI-derived and observed NH$_3$ surface concentrations by NNDMN from 2010 to 2015, the coefficient

343 of the fitted line is 1.03≈1, and the low bias is 2.59%, indicating satellite estimates have good consistency

344 with the measurements. IASI-derived China's NH$_3$ emissions range from 12.17-17.77 Tg N yr^{-1} during

345 2008-2019, among which NH$_3$ emissions increase from 2008 to 2015. The emission intensity of NH$_3$ in

China presents a strong spatial heterogeneity, showing high in the eastern and low in the western. The high values are mainly distributed in the North China Plain and Sichuan Basin. High values are generally distributed in summer, and low values generally occur in winter. This study provides an important reference basis for the formulation of NH_3 pollution prevention and control policy in China.

Data availability

IASI data were obtained from the https://iasi.aeris-data.fr/nh3/. The GIIRS data were obtained from https://zenodo.org/record/4540024.

Author contributions

The study was conceived by LL, and data analysis were performed by JD. The paper was written by PL, with editing from WX and XL. LL was involved in obtaining the project grant and supervised the study.

Competing interests

The contact author has declared that neither they nor their co-authors have any competing interests.

Acknowledgements

This study is supported by the National Natural Science Foundation of China (42001347, 41705130, and 41922037) and the Chinese State Key Research & Development Programme (2017YFC0210100, 2017YFD0200101). The analysis in this study is supported by the Supercomputing Center of Lanzhou University.

References

Clarisse, L., Van Damme, M., Hurtmans, D., Franco, B., Clerbaux, C., and Coheur, P. F.: The diel cycle of NH_3 observed from the FY-4A Geostationary Interferometric Infrared Sounder (GIIRS), Geophys. Res. Lett., 48, e2021GL093010, https://doi.org/10.1029/2021GL093010, 2021.

Cooper, M., Martin, R. V., Padmanabhan, A., and Henze, D. K.: Comparing mass balance and adjoint methods for inverse modeling of nitrogen dioxide columns for global nitrogen oxide emissions, J. Geophys. Res.: Atmos., 122, 4718-4734, https://doi.org/10.1002/2016JD025985, 2017.

Dammers, E., McLinden, C. A., Griffin, D., Shephard, M. W., Graaf, S. V. D., Lutsch, E., Schaap, M., Gainairu-Matz, Y., Fioletov, V., and Damme, M. V.: NH_3 emissions from large point sources derived from CrIS and IASI satellite observations, Atmos. Chem. Phys., 19, 12261-12293, https://doi.org/10.5194/acp-19-12261-2019, 2019.

Dammers, E., Shephard, M. W., Palm, M., Cady-Pereira, K., Capps, S., Lutsch, E., Strong, K., Hannigan, J. W., Ortega, I., Toon, G. C., Stremme, W., Grutter, M., Jones, N., Smale, D., Siemons, J., Hrpcek, K., Tremblay, D., Schaap, M., Notholt, J., and Erisman, J. W.: Validation of the CrIS fast physical NH_3 retrieval with ground-based FTIR, Atmos. Meas. Tech., 10, 2645-2667, https://doi.org/10.5194/amt-10-2645-2017, 2017.

Ding, Y. H., Ren, G. Y., Zhao, Z. C., Xu, Y., Luo, Y., Li, Q. P., and Zhang, J.: Detection, causes and projection of climate change over China: An overview of recent progress, Adv. Atmos. Sci., 24, 954-971, https://doi.org/10.1007/s00376-007-0954-4, 2007.

Dong, W., Xing, J., and Wang, S.: Temporal and spatial distribution of anthropogenic ammonia emissions in China: 1994-2006, Huanjing Kexue, 31, 1457-1463, 2010.

Eastham, S. D., Weisenstein, D. K., and Barrett, S. R.: Development and evaluation of the unified tropospheric–stratospheric chemistry extension (UCX) for the global chemistry-transport model GEOS-Chem, Atmos. Environ., 89, 52-63, https://doi.org/10.1016/j.atmosenv.2014.02.001, 2014.

Flechard, C. R., Nemitz, E., Smith, R. I., Fowler, D., Vermeulen, A. T., Bleeker, A., Erisman, J. W., Simpson, D., Zhang, L., Tang, Y. S., and Sutton, M. A.: Dry deposition of reactive nitrogen to European ecosystems: a comparison of inferential models across the NitroEurope network, Atmos. Chem. Phys., 11, 2703-2728, https://doi.org/10.5194/acp-11-2703-2011, 2011.

Fowler, D., Coyle, M., Skiba, U., Sutton, M. A., Cape, J. N., Reis, S., Sheppard, L. J., Jenkins, A., Grizzetti, B., Galloway, J. N., Vitousek, P., Leach, A., Bouwman, A. F., Butterbach-Bahl, K., Dentener, F., Stevenson, D., Amann, M., and Voss, M.: The global nitrogen cycle in the twenty-first century, Philos. Trans. R. Soc. B-Biol. Sci., 368, 13, https://doi.org/10.1098/rstb.2013.0164, 2013.

Fu, H., Luo, Z., and Hu, S.: A temporal-spatial analysis and future trends of ammonia emissions in China, Sci. Total Environ., 731, 138897, https://doi.org/10.1016/j.scitotenv.2020.138897, 2020.

Geddes, J. A. and Martin, R. V.: Global deposition of total reactive nitrogen oxides from 1996 to 2014 constrained with satellite observations of NO_2 columns, Atmos. Chem. Phys., 17, 10071-10091, https://doi.org/10.5194/acp-17-10071-2017, 2017.

Gilliland, A. B., Dennis, R. L., Roselle, S. J., and Pierce, T. E.: Seasonal NH_3 emission estimates for the eastern United States based on ammonium wet concentrations and an inverse modeling method, J Geophys Res-Atmos, 108, https://doi.org/10.1029/2002jd003063, 2003.

403 Guo, X., Wang, R., Pan, D., Zondlo, M. A., Clarisse, L., Van Damme, M., Whitburn, S., Coheur, P. F.,
404 Clerbaux, C., Franco, B., Golston, L. M., Wendt, L., Sun, K., Tao, L., Miller, D., Mikoviny, T., Müller,
405 M., Wisthaler, A., Tevlin, A. G., Murphy, J. G., Nowak, J. B., Roscioli, J. R., Volkamer, R., Kille, N.,
406 Neuman, J. A., Eilerman, S. J., Crawford, J. H., Yacovitch, T. I., Barrick, J. D., and Scarino, A. J.:
407 Validation of IASI satellite ammonia observations at the pixel scale using in situ vertical profiles, J
408 Geophys Res-Atmos, 126, e2020JD033475, https://doi.org/10.1029/2020jd033475, 2021.
409 He, Y., Pan, Y., Zhang, G., Ji, D., Tian, S., Xu, X., Zhang, R., and Wang, Y.: Tracking ammonia morning
410 peak, sources and transport with 1 Hz measurements at a rural site in North China Plain, Atmos. Environ.,
411 235, 117630, https://doi.org/10.1016/j.atmosenv.2020.117630, 2020.
412 Huang, X., Song, Y., Li, M., Li, J., Huo, Q., Cai, X., Zhu, T., Hu, M., and Zhang, H.: A high-resolution
413 ammonia emission inventory in China, Glob. Biogeochem. Cycle, 26,
414 https://doi.org/10.1029/2011gb004161, 2012.
415 Jacob, D. J.: Introduction to atmospheric chemistry, Princeton University Press1999.
416 Kang, Y., Liu, M., Song, Y., Huang, X., Yao, H., Cai, X., Zhang, H., Kang, L., Liu, X., Yan, X., He, H.,
417 Zhang, Q., Shao, M., and Zhu, T.: High-resolution ammonia emissions inventories in China from 1980
418 to 2012, Atmos. Chem. Phys., 16, 2043-2058, https://doi.org/10.5194/acp-16-2043-2016, 2016.
419 Kong, L., Tang, X., Zhu, J., Wang, Z., Pan, Y., Wu, H., Wu, L., Wu, Q., He, Y., Tian, S., Xie, Y., Liu,
420 Z., Sui, W., Han, L., and Carmichael, G.: Improved inversion of monthly ammonia emissions in China
421 based on the Chinese ammonia monitoring network and ensemble Kalman filter, Environ. Sci. Technol.,
422 53, 12529-12538, https://doi.org/10.1021/acs.est.9b02701, 2019.
423 Kuang, Y., Xu, W., Lin, W., Meng, Z., Zhao, H., Ren, S., Zhang, G., Liang, L., and Xu, X.: Explosive
424 morning growth phenomena of NH_3 on the North China Plain: Causes and potential impacts on aerosol
425 formation, Environ. Pollut., 257, 113621, https://doi.org/10.1016/j.envpol.2019.113621, 2020.
426 Kutzner, R. D., Cuesta, J., Chelin, P., Petit, J.-E., Ray, M., Landsheere, X., Tournadre, B., Dupont, J.-C.,
427 Rosso, A., Hase, F., Orphal, J., and Beekmann, M.: Diurnal evolution of total column and surface
428 atmospheric ammonia in the megacity of Paris, France, during an intense springtime pollution episode,
429 Atmos. Chem. Phys., 21, 12091-12111, https://doi.org/10.5194/acp-21-12091-2021, 2021.
430 Lachatre, M., Fortems-Cheiney, A., Foret, G., Siour, G., Dufour, G., Clarisse, L., Clerbaux, C., Coheur,
431 P.-F., Van Damme, M., and Beekmann, M.: The unintended consequence of SO_2 and NO_2 regulations
432 over China: increase of ammonia levels and impact on PM 2.5 concentrations, Atmos. Chem. Phys., 19,
433 6701-6716, https://doi.org/10.5194/acp-19-6701-2019, 2019.
434 Lamsal, L., Martin, R., Padmanabhan, A., Van Donkelaar, A., Zhang, Q., Sioris, C., Chance, K., Kurosu,
435 T., and Newchurch, M.: Application of satellite observations for timely updates to global anthropogenic
436 NO_x emission inventories, Geophys. Res. Lett., 38, https://doi.org/10.1029/2010GL046476, 2011.
437 Liu, L., Xu, W., Lu, X., Zhong, B., Guo, Y., Lu, X., Zhao, Y., He, W., Wang, S., Zhang, X., Liu, X., and
438 Vitousek, P.: Exploring global changes in agricultural ammonia emissions and their contribution to
439 nitrogen deposition since 1980, P. Natl. Acad. Sci. USA, 119, e2121998119,
440 https://doi.org/10.1073/pnas.2121998119, 2022.
441 Liu, L., Zhang, X., Wong, A. Y., Xu, W., Liu, X., Li, Y., Mi, H., Lu, X., Zhao, L., Wang, Z., Wu, X., and
442 Wei, J.: Estimating global surface ammonia concentrations inferred from satellite retrievals, Atmos.
443 Chem. Phys., 19, 12051-12066, https://doi.org/10.5194/acp-19-12051-2019, 2019.

Ma, S.: High-resolution assessment of ammonia emissions in China: Inventories, driving forces and mitigation, Atmos. Environ., 229, 117458, https://doi.org/10.1016/j.atmosenv.2020.117458, 2020.

Marais, E. A., Pandey, A. K., Van Damme, M., Clarisse, L., Coheur, P. F., Shephard, M. W., Cady-Pereira, K. E., Misselbrook, T., Zhu, L., Luo, G., and Yu, F.: UK Ammonia Emissions Estimated With Satellite Observations and GEOS-Chem, J Geophys Res-Atmos, 126, e2021JD035237, https://doi.org/10.1029/2021JD035237, 2021.

Paerl, H. W., Gardner, W. S., McCarthy, M. J., Peierls, B. L., and Wilhelm, S. W.: Algal blooms: noteworthy nitrogen, Science, 346, 175-175, https://doi.org/10.1126/science.346.6206.175-a, 2014.

Pan, Y., Tian, S., Zhao, Y., Zhang, L., Zhu, X., Gao, J., Huang, W., Zhou, Y., Song, Y., and Zhang, Q.: Identifying ammonia hotspots in China using a national observation network, Environ. Sci. Technol., 52, 3926-3934, https://doi.org/10.1021/acs.est.7b05235, 2018.

Pandolfi, M., Amato, F., Reche, C., Alastuey, A., Otjes, R. P., Blom, M. J., and Querol, X.: Summer ammonia measurements in a densely populated Mediterranean city, Atmos. Chem. Phys., 12, 7557-7575, https://doi.org/10.5194/acp-12-7557-2012, 2012.

Paulot, F., Jacob, D. J., Pinder, R. W., Bash, J. O., Travis, K., and Henze, D. K.: Ammonia emissions in the United States, European Union, and China derived by high-resolution inversion of ammonium wet deposition data: Interpretation with a new agricultural emissions inventory (MASAGE_NH3), J. Geophys. Res.-Atmos., 119, 4343-4364, https://doi.org/10.1002/2013jd021130, 2014.

Peng, S., Huang, J., Zhong, X., Yang, J., Wang, G., Zou, Y., Zhang, F., Zhu, Q., Buresh, R., and Witt, C.: Challenge and opportunity in improving fertilizer-nitrogen use efficiency of irrigated rice in China, Agric. Sci. China, 1, 776-785, 2002.

Pinder, R. W., Walker, J. T., Bash, J. O., Cady-Pereira, K. E., Henze, D. K., Luo, M. Z., Osterman, G. B., and Shephard, M. W.: Quantifying spatial and seasonal variability in atmospheric ammonia with in situ and space-based observations, Geophys. Res. Lett., 38, 5, https://doi.org/10.1029/2010gl046146, 2011.

Shephard, M. W. and Cady-Pereira, K. E.: Cross-track Infrared Sounder (CrIS) satellite observations of tropospheric ammonia, Atmos. Meas. Tech., 8, 1323-1336, https://doi.org/10.5194/amt-8-1323-2015, 2015.

Someya, Y., Imasu, R., Shiomi, K., and Saitoh, N.: Atmospheric ammonia retrieval from the TANSO-FTS/GOSAT thermal infrared sounder, Atmos. Meas. Tech., 13, 309-321, https://doi.org/10.5194/amt-13-309-2020, 2020.

Van Damme, M., Whitburn, S., Clarisse, L., Clerbaux, C., Hurtmans, D., and Coheur, P.-F.: Version 2 of the IASI NH$_3$ neural network retrieval algorithm: near-real-time and reanalysed datasets, Atmos. Meas. Tech., 10, 4905-4914, https://doi.org/10.5194/amt-10-4905-2017, 2017.

Van Damme, M., Clarisse, L., Whitburn, S., Hadji-Lazaro, J., Hurtmans, D., Clerbaux, C., and Coheur, P. F.: Industrial and agricultural ammonia point sources exposed, Nature, 564, 99-103, https://doi.org/10.1038/s41586-018-0747-1, 2018.

Van Damme, M., Clarisse, L., Heald, C. L., Hurtmans, D., Ngadi, Y., Clerbaux, C., Dolman, A., Erisman, J. W., and Coheur, P.-F.: Global distributions, time series and error characterization of atmospheric ammonia (NH$_3$) from IASI satellite observations, Atmos. Chem. Phys., 14, 2905-2922, https://doi.org/10.5194/acp-14-2905-2014, 2014.

Wang, S., Nan, J., Shi, C., Fu, Q., Gao, S., Wang, D., Cui, H., Saiz-Lopez, A., and Zhou, B.: Atmospheric ammonia and its impacts on regional air quality over the megacity of Shanghai, China, Sci. Rep.-UK, 5, 1-13, https://doi.org/10.1038/srep15842, 2015.

Wang, Z., Zhang, X., Liu, L., Cheng, M., and Xu, J.: Spatial and seasonal patterns of atmospheric nitrogen deposition in North China, Atmospheric and Oceanic Science Letters, 13, 188-194, https://doi.org/10.1080/16742834.2019.1701385, 2020.

Warner, J. X., Wei, Z. G., Strow, L. L., Dickerson, R. R., and Nowak, J. B.: The global tropospheric ammonia distribution as seen in the 13-year AIRS measurement record, Atmos. Chem. Phys., 16, 5467-5479, https://doi.org/10.5194/acp-16-5467-2016, 2016.

Werner, M., Kryza, M., Geels, C., Ellermann, T., and Skjøth, C. A.: Ammonia concentrations over Europe–application of the WRF-Chem model supported with dynamic emission, Pol. J. Environ. Stud., 26, 1323-1341, https://doi.org/10.15244/pjoes/67340, 2017.

Wesely, M.: Parameterization of surface resistances to gaseous dry deposition in regional-scale numerical models, Atmos. Environ., 41, 52-63, https://doi.org/10.1016/j.atmosenv.2007.10.058, 2007.

Whitburn, S., Van Damme, M., Clarisse, L., Bauduin, S., Heald, C., Hadji-Lazaro, J., Hurtmans, D., Zondlo, M. A., Clerbaux, C., and Coheur, P. F.: A flexible and robust neural network IASI-NH_3 retrieval algorithm, J Geophys Res-Atmos, 121, 6581-6599, https://doi.org/10.1002/2016JD024828, 2016.

Xu, W., Luo, X. S., Pan, Y. P., Zhang, L., Tang, A. H., Shen, J. L., Zhang, Y., Li, K. H., Wu, Q. H., Yang, D. W., Zhang, Y. Y., Xue, J., Li, W. Q., Li, Q. Q., Tang, L., Lu, S. H., Liang, T., Tong, Y. A., Liu, P., Zhang, Q., Xiong, Z. Q., Shi, X. J., Wu, L. H., Shi, W. Q., Tian, K., Zhong, X. H., Shi, K., Tang, Q. Y., Zhang, L. J., Huang, J. L., He, C. E., Kuang, F. H., Zhu, B., Liu, H., Jin, X., Xin, Y. J., Shi, X. K., Du, E. Z., Dore, A. J., Tang, S., Collett, J. L., Goulding, K., Sun, Y. X., Ren, J., Zhang, F. S., and Liu, X. J.: Quantifying atmospheric nitrogen deposition through a nationwide monitoring network across China, Atmos. Chem. Phys., 15, 12345-12360, https://doi.org/10.5194/acp-15-12345-2015, 2015.

Zhang, L., Chen, Y. F., Zhao, Y. H., Henze, D. K., Zhu, L. Y., Song, Y., Paulot, F., Liu, X. J., Pan, Y. P., Lin, Y., and Huang, B. X.: Agricultural ammonia emissions in China: reconciling bottom-up and top-down estimates, Atmos. Chem. Phys., 18, 339-355, https://doi.org/10.5194/acp-18-339-2018, 2018.

Zhang, X., Wu, Y., Liu, X., Reis, S., Jin, J., Dragosits, U., Van Damme, M., Clarisse, L., Whitburn, S., Coheur, P.-F. o., and Gu, B.: Ammonia emissions may be substantially underestimated in China, Environ. Sci. Technol., 51, 12089-12096, https://doi.org/10.1021/acs.est.7b02171, 2017.

Zhang, X. M., Ren, C. C., Gu, B. J., and Chen, D. L.: Uncertainty of nitrogen budget in China, Environ. Pollut., 286, 9, https://doi.org/10.1016/j.envpol.2021.117216, 2021.

Zhang, Y., Liu, X., Zhang, F., Ju, X., Zou, G., and Hu, K.: Spatial and temporal variation of atmospheric nitrogen deposition in the North China Plain, Acta Ecologica Sinica, 26, 1633-1638, https://doi.org/10.1016/S1872-2032(06)60026-7, 2006.

Zhou, F., Ciais, P., Hayashi, K., Galloway, J., Kim, D.-G., Yang, C., Li, S., Liu, B., Shang, Z., and Gao, S.: Re-estimating NH_3 emissions from Chinese cropland by a new nonlinear model, Environ. Sci. Technol., 50, 564-572, https://doi.org/10.1021/acs.est.5b03156, 2016.